

A thermocatalytic perovskite-graphene oxide nanofiltration membrane for water depollution

Bortot Coelho, Fabrício E.; Nurisso, Federica; Boffa, Vittorio; Ma, Xianzheng; Rasse-Suriani, Federico A. O.; Roslev, Peter; Magnacca, Giuliana; Deganello, Francesca ; La Parola, Valera

Published in:
Journal of Water Process Engineering

DOI (link to publication from Publisher):
[10.1016/j.jwpe.2022.102941](https://doi.org/10.1016/j.jwpe.2022.102941)

Creative Commons License
CC BY 4.0

Publication date:
2022

Document Version
Publisher's PDF, also known as Version of record

[Link to publication from Aalborg University](#)

Citation for published version (APA):
Bortot Coelho, F. E., Nurisso, F., Boffa, V., Ma, X., Rasse-Suriani, F. A. O., Roslev, P., Magnacca, G., Deganello, F., & La Parola, V. (2022). A thermocatalytic perovskite-graphene oxide nanofiltration membrane for water depollution. *Journal of Water Process Engineering*, 49(49), Article 102941. <https://doi.org/10.1016/j.jwpe.2022.102941>

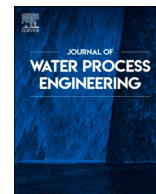
General rights

Copyright and moral rights for the publications made accessible in the public portal are retained by the authors and/or other copyright owners and it is a condition of accessing publications that users recognise and abide by the legal requirements associated with these rights.

- Users may download and print one copy of any publication from the public portal for the purpose of private study or research.
- You may not further distribute the material or use it for any profit-making activity or commercial gain
- You may freely distribute the URL identifying the publication in the public portal -

Take down policy

If you believe that this document breaches copyright please contact us at vbn@aub.aau.dk providing details, and we will remove access to the work immediately and investigate your claim.



A thermocatalytic perovskite-graphene oxide nanofiltration membrane for water depollution

Fabricio E. Bortot Coelho^{a,b}, Federica Nurisso^{a,c}, Vittorio Boffa^{c,*}, Xianzheng Ma^c,
Federico A.O. Rasse-Suriani^{c,d}, Peter Roslev^c, Giuliana Magnacca^a, Victor Candelario^b,
Francesca Deganello^e, Valeria La Parola^e

^a Dipartimento di Chimica and NIS Interdepartmental Centre, Università di Torino, Via P. Giuria 7, 10125 Torino, Italy

^b Liqtech International A/S, Industriparken 22 C, DK-2750 Ballerup, Denmark

^c Center for Membrane Technology, Department of Chemistry and Bioscience, Aalborg University, Fredrik Bajers Vej 7H, DK-9220 Aalborg East, Denmark

^d Instituto de Investigaciones Físicoquímicas Teóricas y Aplicadas, Departamento de Química, Universidad Nacional de La Plata, Diag 113 y 64, La Plata, Argentina

^e Istituto per lo Studio dei Materiali Nanostrutturati, Consiglio Nazionale delle Ricerche, Via Ugo La Malfa 153, 90146 Palermo, Italy

ARTICLE INFO

Keywords:

Nanocomposite
Strontium ferrate
Wastewater
Contaminants of emerging concern
Toxicological tests

ABSTRACT

A novel nanofiltration membrane, whose active layer consists of 98.6 wt% of a thermocatalytic perovskite with composition $\text{Sr}_{0.85}\text{Ce}_{0.15}\text{FeO}_{3.8}$ (CSF), 1.0 wt% of graphene oxide (GO), and 0.4 wt% of a humic acid-like (HAL) crosslinker, was deposited over a commercial flat-sheet polyethersulfone support with good reproducibility by a simple 1-step coating procedure. The synergistic coupling of CSF and the crosslinked GO resulted in an improved catalytic activity for bisphenol A (BPA) abatement as a model pollutant. The thermocatalytic CSF/GO/HAL (GOT) membrane was tested in a nanofiltration crossflow apparatus with a model BPA solution and with a real urban wastewater treatment plant effluent. Its performances were compared with those of a HAL crosslinked GO (GOHAL) reference membrane. The GOT membrane presented high rejection towards BPA, antifouling properties, and stability under the filtration conditions. Moreover, when compared to the GOHAL reference, the thermocatalytic GOT membrane was able to reduce the concentration of BPA and the total organic carbon in the feed during filtration. Hence, the GOT membrane appears to have high potential in water treatment due to its multifunctional characteristics, which include molecular sieving, thermocatalytic oxidation of organic pollutants, and self-cleaning properties. Additionally, the membrane material showed no significant toxicity to the aquatic model organisms *Raphidocelis subcapitata*, *Aliivibrio fischeri*, and *Daphnia magna* at concentrations below 50 ppm.

1. Introduction

In recent years, an increasing number of organic contaminants of emerging concern (CECs) has been found in natural water systems [1–3]. These water pollutants, which include pharmaceuticals, industrial auxiliaries, pesticides, and consumer products, cannot be fully degraded by the conventional physical and biological treatments, and therefore they are eventually discharged into the aquatic environment. Although the concentrations of these CECs typically do not exceed the $\mu\text{g L}^{-1}$ level, they can be potentially harmful to aquatic life in receiving waters [4,5]. Moreover, CECs and their chemical or biological transformation products can enter the food chain or contaminate drinking water resources, with a potentially negative impact on human health [6,7]. In this context, advanced oxidation processes (AOPs) are attractive tertiary

treatment options for the abatement of CECs in urban and industrial wastewater streams, thus mitigating the problem of their release into the environment [8]. AOPs are based on the in-situ production of strong oxidants, such as hydroxyl and superoxide radicals, for the fast oxidation of CECs. Ozonation and UV-C treatments [9–11] are established AOPs for the depollution and disinfection of wastewater, drinking water, and water in recirculated systems (e.g. recirculated aquaculture systems [12,13]). Besides them, other AOPs, such as Fenton-based processes [14,15], and photocatalytic abatement by ceramic semiconductors (e.g. titanium dioxide) [16,17] are emerging as highly promising methods for CECs removal from wastewaters. However, these technologies rely on the addition of chemicals and/or light exposure.

Among ceramic materials, certain perovskites have been recently reported to promote the advanced oxidation of organic pollutants in

* Corresponding author.

E-mail address: vb@bio.aau.dk (V. Boffa).

<https://doi.org/10.1016/j.jwpe.2022.102941>

Received 23 March 2022; Received in revised form 7 June 2022; Accepted 11 June 2022

Available online 28 June 2022

2214-7144/© 2022 The Authors. Published by Elsevier Ltd. This is an open access article under the CC BY license (<http://creativecommons.org/licenses/by/4.0/>).

wastewater [18–23] without chemical additives and under dark conditions. The degradation mechanisms that are involved in this thermocatalytic process have not been clarified yet. According to Chen et al. [22], surface electron transfer (SET) is the most probable mechanism for the oxidation of organic pollutants by these perovskites under dark conditions. Based on SET, the ceramic thermocatalyst acts as an “electron tunnel” by transferring electrons from the adsorbed organic contaminants to the adsorbed oxygen species, thus degrading organics and forming reactive oxygen species, which can further react with the dissolved organic compounds. For instance, strontium ferrate and Ce-doped strontium ferrate were observed being effective in degrading various model pollutants, e.g. bisphenol A, acid orange 7, acid orange 8, and acetamiprid [23,24], under dark conditions. Moreover, we have recently coupled the thermocatalytic abatement of organic pollutants by a perovskite with nominal composition $\text{Sr}_{0.85}\text{Ce}_{0.15}\text{FeO}_{3-\delta}$, hereinafter named CSF, with membrane technology, as a separate step for the degradation of organic pollutants in the membrane concentrate [24,25]. Integration of CSF with membrane distillation [24] allowed drawing of clean water at the cold side (permeate) of the membrane, while simultaneously degrading organics concentrated at the hot side of the membrane. Therefore, thermal energy, which can be taken from renewable or waste heat sources, drives water permeation through the membrane and the same time activates CSF for the thermocatalytic degradation of CECs. In a different study [25], we combined CSF thermocatalysis under dark conditions with an Al_2O_3 -doped silica nanofiltration tubular membrane [26] in two ways: (i) addition of CSF at the membrane feed during filtration allowed for CECs abatement, while mitigating membrane fouling and improving the quality of permeate of the NF membrane, which did not show complete rejection of CECs; (ii) pre-concentration of the wastewater by nanofiltration allowing for a strong reduction of the thermal energy needed for CECs abatement by CSF. These two CSF-membrane concepts were shown to be effective in the production of pure water without creating a toxic concentrate and with no need for additional chemicals or light sources.

Within the current trend of process intensification, the possibility to integrate the selective CECs rejection of NF with the advanced oxidation of contaminants in a single functional membrane is highly attractive, in reason of the numerous benefits resulting from the synergistic integration of these two technologies [27]. Thus, different functional NF membrane concepts, in which contaminant oxidation is performed by photocatalytic materials [28,29] or enzymes immobilized on the membrane surface [30,31], have been proposed in the past years. An obvious advantage of these devices is that the immobilization of the biocatalyst or photocatalyst over the membrane surface solves the problem of its recovery. Moreover, synergistic interaction between the catalyst and the membrane matrix can increase degradation rates. For instance, a few TiO_2 -functionalized graphene oxide (GO) membranes have been recently reported [32–36]. These membranes combine the well-known photocatalytic activity of TiO_2 nanoparticles [37] with the ability of GO films to provide CECs rejection in the NF range [38–42]. Moreover, the chemical interaction between TiO_2 and GO is beneficial for CECs abatement, by extending the light absorption spectrum of the ceramic photocatalyst to the visible light, by hindering electron-hole pair recombination, and because organic contaminants are adsorbed by GO near the photocatalytic centers where reactive oxygen species are formed. At the same time, the formation of reactive oxygen species over the membrane surface can mitigate fouling, thus extending the service time between cleaning cycles. The development of such photocatalytic membranes implies solving several challenges concerning membrane fabrication and unit design [27]. Furthermore, photocatalytic membranes might not be suitable for all water systems, because turbidity might hinder the photocatalytic process. On the other hand, oxidation of organic contaminants under dark conditions was achieved by immobilization of enzymes (e.g., laccase [43,44]) on the surface of NF membranes, although these biocatalytic NF membranes are difficult to clean and their service time is limited due to the intrinsic fragility of the

biocatalysts.

In response to the above-described drawbacks of the photocatalytic and the enzymatic membranes for water depollution, here we present a new type of nanofiltration membrane, which can simultaneously retain and degrade CECs by means of the thermocatalytic perovskite CSF. The membrane was prepared via a facile procedure, and its functioning does not require light or additional chemicals. CSF ceramic powder is typically synthesized by the solution-combustion method and calcined at 1000 °C to obtain the active cubic crystal structure [45]. It consists of flake-shaped dense particles with lateral dimensions ranging from 1 to 30 μm and thickness smaller than 0.2 μm [24]. Such ceramic particles are not suited to fabricate ceramic membrane layers with pore size in the micropore range (which is needed to achieve CECs rejection) by the typical powder dispersion dip-coating procedures. Therefore, we used a completely different approach in this work. The CSF powder (98.6 wt%) was embedded in a crosslinked GO matrix (1.4 wt%) to obtain a stable NF membrane layer. A waste-derived humic acid-like (HAL) biopolymer was used as a crosslinker, because it was shown to be highly effective in providing stability to GO against exfoliation [46–48]. HAL was obtained from a renewable source, and it is inexpensive and non-toxic. The CSF-GO-HAL composite was deposited on top of a commercial polymeric ultrafiltration flat-sheet support. Even when used at loading as low as 1.4 wt%, crosslinked GO allowed to obtain a CSF membrane with selectivity in the NF range and stable in our crossflow filtration tests. The membrane was tested with the model industrial wastewater pollutant, bisphenol a (BPA), and with a real wastewater effluent, to investigate the ability of the membrane to retain and degrade water pollutants and to mitigate fouling. The synergistic interaction between GO and CSF was investigated with batch abatement experiments. Moreover, the potential toxicity of CSF particles following a possible release into the environment was tested with aquatic model organisms.

2. Materials and methods

All the chemicals used in this work were purchased from Sigma–Aldrich unless otherwise specified. The deionized water had a resistivity higher than 18 $\text{M}\Omega\text{ cm}^{-1}$. Wastewater secondary effluent was sampled from the wastewater treatment plant in Aalborg West (57.049422° N, 9.864735° E), Denmark. The samples were cooled at 5 °C within 1 h after collection and kept at this temperature until used for the filtration experiments. The thermocatalytic perovskite (CSF) was prepared by the solution-combustion synthesis [23], the graphene oxide (GO) dispersion according to a modified Hummers' method [46], and the crosslinker (HAL) and by Montoneri's extraction procedure [49]. OriginPro 2021 (OriginLab Corporation, Northampton, MA USA) was used to analyze data, prepare graphs, and perform iterative non-linear regressions and calculations of 95 % confidence limits for abatement tests and EC50 values.

2.1. CSF synthesis

1.80 g strontium nitrate anhydrous (AVOCADO Research Chemicals Ltd., 99 %), 4.04 g iron (III) nitrate nonahydrate (98 %) and 0.65 g cerium (III) nitrate hexahydrate (99 %), 7.68 g citric acid (99.5 %), and 9.25 g of ammonium nitrate (99.5 %) were dissolved in 200 mL of deionized water. The pH of the solution was adjusted to 6.0 using ammonium hydroxide (25 wt%) and the glass beaker was placed on the hot plate and kept at 80 °C for the evaporation of the water under continuous magnetic stirring. After obtaining a sticky gel, the hot plate was set to the maximum temperature (310 °C) to start the gel self-ignition. After the combustion, the as-burned powder was calcined at 1000 °C for 5 h with a heating rate of 5 °C min^{-1} . After calcination, about 2 g of $\text{Sr}_{0.85}\text{Ce}_{0.15}\text{FeO}_{3-\delta}$ powder were obtained.

2.2. Preparation of the stock GO dispersion

2.0 g of natural graphite (Graphit Kropfmühl GmbH) and 1.0 g of sodium nitrate (99 %) were added to 50 mL of 98 % sulfuric acid under vigorous stirring, while the temperature of the mixture was kept at 0 °C by an ice bath. 7.0 g of potassium permanganate was added to the suspension slowly to prevent a sudden temperature increase. After stirring the mixture was stirred for 10 min, the reaction flask was placed into a water bath at 35 °C for 1 h and a thick dark green paste was obtained. The paste was slowly poured into 80 mL deionized water and a dark brown suspension was obtained. After adding 500 mL of deionized water, followed by 6 mL of 30 % H₂O₂ solution, the mixture color changed into light yellow. After that, the suspension was washed with 200 mL HCl (5 %) one time, and with 500 mL deionized water 5 times. The absence of sulfates in the mixture was confirmed by the barium chloride test. The dispersion was diluted with deionized water to obtain a GO concentration of 28 g L⁻¹. This stock GO dispersion was used for the synthesis of the nanocomposite powders and membranes.

2.3. Preparation of the stock crosslinker solution

The humic acid-like crosslinker (HAL) was isolated from green compost produced at ACEA Pinerolese Industriale S.p.A. waste treatment plant in Pinerolo, Italy, according to a procedure reported elsewhere procedure [49,50]. The green compost was obtained from the collection of urban public park trimmings and home gardening residues aged for >180 days. HAL was isolated by treating 50 g of the green compost with 1 L of 6 M aqueous NaOH under stirring at 60 °C for 4 h. The extracted liquid phase was then separated from the solid waste by centrifugation and concentrated over an ultrafiltration membrane (MWCO = 5KDa). The retentate fraction was then dried at 60 °C for 24 h to give a black solid. The so obtained potassium salt of HAL was dissolved in water to obtain a stock solution with a crosslinker concentration of 11.2 g L⁻¹.

2.4. Membrane fabrication

The stock GO dispersion was mixed with the crosslinker solution to reach a GOHAL mixture with HAL/GO weight ratio of 0.4. The CSF powder was ground in a mortar, dispersed in deionized water (10 g L⁻¹), and then ultrasonicated for 30 min. The dispersed CSF was added in the GOHAL mixture to obtain membrane materials with CSF loading of 0 wt %, 26 wt%, 93 wt%, 97.2 wt%, and 98.6 wt%. After adding 5 µL of concentrated HCl (37 wt%) for each milliliter of CSF/GO/HAL dispersion to promote crosslinking between GO and HAL, the final mixture was stirred for 4 h and directly used for membrane fabrication. A polyethersulfone (PES) ultrafiltration membrane (MWCO = 100 kDa, Synder Filtration, Vacaville, CA USA) was selected as support for the thermocatalytic perovskite-graphene oxide nanocomposite films. Before coating, the support was soaked in water overnight to remove chemical impurities from its surface and then dried in air for one day. Thermocatalytic perovskite-graphene oxide supported on flat-sheet polyethersulfone membrane (hereafter referred to as "GOT membranes") were prepared by Meyer rod-coating with a wire bare coater with 50 µm modulation and application length of 320 mm (Industrial Physics Inks & Coatings B.V., Capelle aan den IJssel, The Netherlands). After coating the supported membranes were dried in the air and cured in a vacuum oven at 80 °C overnight. Unsupported membrane materials for XRD and HRTEM analyses and the toxicological tests were obtained by drying the CSF/GO/HAL dispersions in the air and following the same curing procedure used for the supported GOT membranes.

2.5. Materials characterization

X-ray diffraction (XRD) measurements were performed on a PANalytical Empyrean diffractometer, operating at 45 kV and 40 mA, with

Cu Kα radiation. Sr_{0.85}Ce_{0.15}FeO_{3-δ} was indexed in the Inorganic Crystal Structure Database (ICSD) under code #249012. Membrane structure was observed at SEM (ZEISS EVO 50 XVP microscope) with LaB6 source. The samples were mounted on metallic stubs with double-sided conductive tape and ion coated with a 5 nm chromium layer to avoid any charging effect. The chemical composition of samples was analyzed by Energy-Dispersive Spectroscopy (EDS) using Oxford EDS INCA (Oxford Instruments). High-resolution transmission electron microscopy (HRTEM) images were obtained on a JEOL 3010-UHR instrument. The X-ray photoelectron spectroscopy (XPS) analyses were performed with a VGMicrotech ESCA 3000Multilab, equipped with a dual Mg/Al anode. The spectra were excited by the monochromatized Al Kα source (1486.6 eV) run at 14 kV and 15 mA. The analyzer was operated in the constant analyzer energy (CAE) mode. For the individual peak energy regions, pass energy of 20 eV set across the hemispheres was used. Survey spectra were measured at 50 eV pass energy.

2.6. Thermocatalytic abatement tests and water analysis

200 mL of bisphenol A (BPA) solution (10 mg L⁻¹ in deionized water) was poured in a 500 mL three-neck round bottom flask immersed in an oil bath. The solution was heated under reflux to 50 °C. Then, the powdered membrane material was added to reach a concentration of 0.5 g L⁻¹ and the pH was adjusted to 7.0. The solution was continuously stirred and sampled at regular time intervals. The collected samples were filtered over 0.45 µm syringe filters and analyzed by HPLC (Summit-Dionex, with a Luna 5 µ C18 100 Å column (250 × 4.60 mm), mobile phase (isocratic acetonitrile/water = 60/40) flow of 1 mL min⁻¹, UV detector at 230 nm) to determine BPA concentration. Total organic carbon (TOC) analysis was performed on a VarioTOC (Elementar, Hanau, Germany).

2.7. Filtration tests

Crossflow filtration tests were performed on flat sheets membranes (filtration area 25 cm²) in a lab-made NF apparatus reported elsewhere [51]. In brief, the setup consists of a NF module connected with a high-pressure pump (BEVI, IEC 34-1, Sweden), which controls the pressure of the membrane feed, and a rotary lobe pump (Philipp Hilge GmbH & Co., Novalobe 60/1.90, Germany), which controls the crossflow velocity. Two pressure transmitters (Danfoss, MBS 4010, Nordborg Denmark) are present at the module inlet and outlet. The mass flow of the permeate was measured by a balance (Mettler Toledo, Mono Bloc series, Switzerland) connected to a computer. Tests started by filling up the feed tank with 1.8 L. The apparatus was operated at a transmembrane pressure difference of 5.0 bar, with a pumped water flux of around 4 × 10⁻⁶ m³ s⁻¹, and a feed temperature of 50 °C. The membrane permeability was measured by a balance placed below the permeate beaker. During filtration, samples were collected from feed and permeate at various times. Membrane selectivity was calculated based on the concentration of BPA in the permeate and in the feed, according to Eq. (1):

$$\text{selectivity} = 1 - \frac{C_{\text{permeate}}}{C_{\text{feed}}} \quad (1)$$

2.8. Toxicological tests

Toxicity tests were carried out to assess the potential ecotoxicity of CSF particles if accidentally released into the environment. The test included the aquatic model organisms *Aliivibrio fischeri*, *Raphidocelis subcapitata* and *Daphnia magna*. Dispersions of CSF in aqueous solutions were prepared using sonication (Qsonica Q55, Newtown CT, USA). Toxicity test with the luminescent bacterium *A. fischeri* and the unicellular green microalgae *R. subcapitata* (formerly *Pseudokirchneriella subcapitata*) was carried out partly as described by Papagiannaki et al. [52]. *A. fischeri* DSM 7151 was incubated in white 96-well plates (CulturPlate,

Perkin Elmer) on a microshaker at 200 rpm in the presence of 10 different concentrations of CSF ($n = 8$). Changes in bioluminescence were quantified after 30 min using a Victor X2 Multilabel Plate Reader (Perkin Elmer). *R. subcapitata* was incubated in 96-well clear Nunclon microplates (Thermo Scientific) on a shaker at 40 rpm with illumination (6500 lx) in the presence of 10 different concentrations of CSF ($n = 8$). The endpoint was inhibition of growth measured as absorbance using a Thermo Multiskan Plate Reader (Thermo Scientific). Acute toxicity and starvation survival of the crustacean *D. magna* was carried out partly as described by Nielsen and Roslev [53]. *D. magna* was incubated in 24-well clear microplates with one animal per well (2 mL) in darkness in the presence of 3 different concentrations of CSF ($n = 24$), in triplicate. The endpoint for acute toxicity (24 h and 48 h) was inhibition of mobility whereas the endpoint for starvation-survival was death defined as the complete absence of movement (body, antennae, filtration apparatus). Acute toxicity and starvation survival were expressed as inhibition (I) relative to control samples: $I = 1 - (R_i / R_c)$ where R_i and R_c are responses measured for inhibited and control samples, respectively. Concentration-response curves were fitted to a Log-logistic model using iterative non-linear regression:

$$Response = A1 + \frac{A2 - A1}{1 + 10^{(Log X - C)p}} \quad (2)$$

where A1 is the bottom asymptote, A2 is the top asymptote, X represents the median effective concentration (EC50), C is the CSF concentration (mg L^{-1}), and p is a model parameter representing the slope of the curve. Median starvation survival time (SS50) for *D. magna* was calculated from non-linear regression and a sigmoidal survival curve [53].

3. Results and discussion

3.1. GOT nanocomposites

XRD patterns of CSF/GO/HAL nanocomposites (GOT nanocomposites) with different perovskite content are shown in Fig. 1a. The diffractogram of the starting GO powder shows a main peak at $11.33^\circ 2\theta$, which corresponds to an interlayer distance of 7.79 Å and to an O/C atomic ratio of about 0.27 in agreement with the literature [54]. The presence of a single peak in this diffractogram is consistent with the layered structure shown by the TEM micrograph in Fig. 1b. These stacked structures disappear upon crosslinking with HAL, and the diffractogram of GOHAL indicates a highly disordered material, as confirmed by the TEM image in Fig. 1c. Indeed, it was already observed that upon crosslinking and thermal stabilization, HAL brings a high degree of disorder in GO materials, which preserves the membrane permeability preventing the formation of dense graphitic domains and reducing the tortuosity of the permeation path of the water molecules across the membrane [46]. The low-intensity peak at about $26^\circ 2\theta$ in the GOHAL diffractogram can be ascribed to the formation of small graphitic domains during the curing of the material at 80°C [55]. The angular range of the perovskite CSF, $30\text{--}85^\circ 2\theta$ does not overlap with those of GO and GOHAL, which are instead concentrated between 5° and $30^\circ 2\theta$. This allows noticing the presence of CSF in the GOT nanocomposites without disturbance. The relative intensities of the perovskite signals decrease with the decrement of the CSF component in the formulation from the nanocomposite with 98.6 % of GO loading (GOT_98.6 %) to the nanocomposite with 26 % of CSF loading (GOT_26%). Pure CSF contains traces (about 1 wt%) of CeO_2 , as already observed in the literature [23]. The perovskite phase structure and microstructure seem not to be

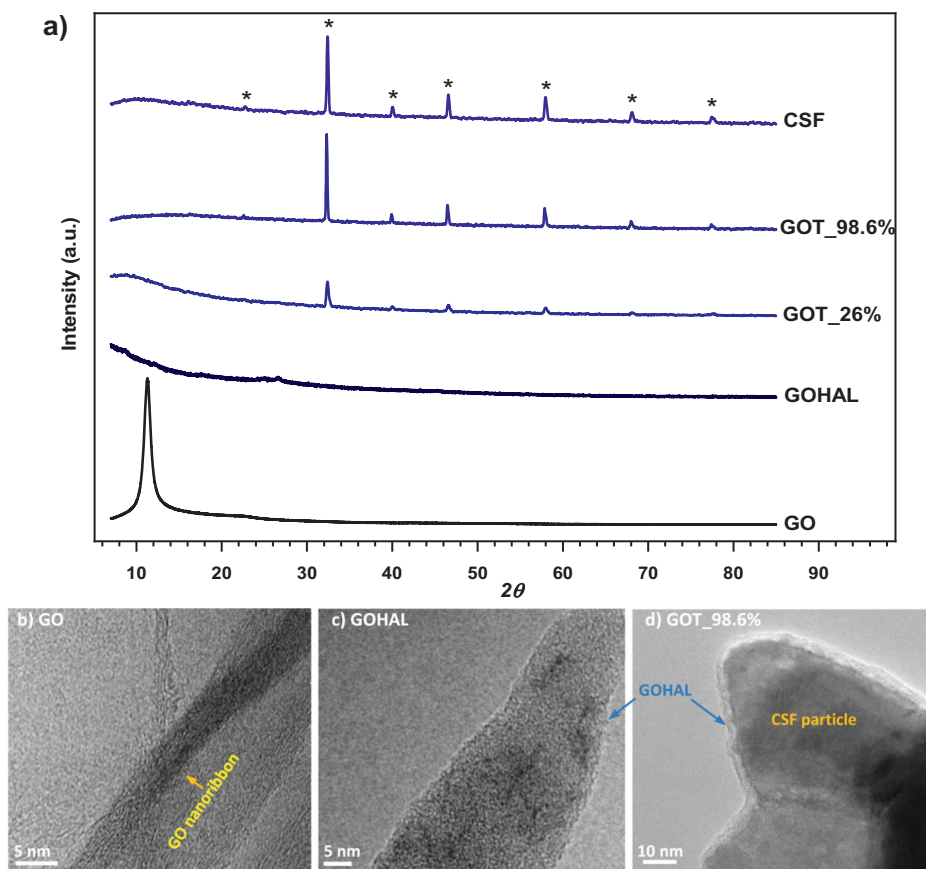


Fig. 1. Morphology of GOT nanocomposites: (a) XRD diffractograms of selected GOT materials and of their components graphene oxide (GO), HAL crosslinked GO (GOHAL), and thermocatalytic perovskite (CSF), where the symbols (*) indicate the characteristic peaks of CSF; HR-TEM micrographs of (b) GO, (c) GOHAL, and (d) GOT_98.6 % powders.

altered by the presence of GO in the formulation. The TEM micrograph in Fig. 1d shows the close contact of the GOHAL matrix with CSF in GOT_98.6 %. This type of interface is desirable for the synergistic interaction between the GO-based matrix and the ceramic semiconductor for the abatement of water contaminants [56,57].

3.2. CSF-GO synergism in the abatement of bisphenol A

The potential synergism between GO and CSF was investigated by testing the thermocatalytic degradation of bisphenol A (BPA), as a model pollutant, by GOT nanocomposites at 50 °C. GOHAL powders were loaded with 26 wt%, 93 wt%, 97.2 wt%, and 98.6 wt% of CSF, and named in Fig. 2 after GOT_26%, GOT_93%, GOT_97.2 %, and GOT_98.6 %, respectively. Moreover, the same test was performed with the pure GOHAL and CSF powders as references. The BPA normalized concentration (C/C_0) as a function of the test time is plotted for the different membrane materials in Fig. 2a. As expected, GOHAL alone cannot achieve the abatement of BPA (50 ppm in deionized water), which is instead degraded by CSF (45 % BPA abatement in 2 h). The GOT_98.6 % nanocomposite achieves 52 % BPA abatement in 2 h, indicating a synergistic interaction between GO and CSF, as already reported for other catalytic and photocatalytic semiconductor ceramics [58,59]. On the other hand, when the CSF loading is reduced to 93 wt% (GOT_93% powder) <20 wt% of BPA is degraded in 2 h. In order to highlight the impact of the material composition on the thermocatalytic performances, the kinetic constants (k) of the thermocatalytic degradation of BPA by GOT nanocomposites were calculated according to a pseudo-first order reaction mechanism and plotted in Fig. 2b as a function of the CSF loading in the membrane material. The sample with 98.6 % CSF loading shows the highest abatement rate constant: $(6.2 \pm 0.3) \times 10^{-3} \text{ min}^{-1}$; while the pure CSF powder has $k = (5.2 \pm 0.1) \times 10^{-3} \text{ min}^{-1}$. However, k declines with decreasing CSF loading, i.e. increasing the amount of GOHAL in the material. Indeed, the kinetic constants decreased to $(1.89 \pm 0.08) \times 10^{-3}$, $(1.72 \pm 0.05) \times 10^{-3}$, and $(1.6 \pm 0.9) \times 10^{-4} \text{ min}^{-1}$ for GOT nanocomposites with a CSF loading of 97.3 wt%, 93 wt%, and 26 wt%, respectively. This trend can be explained by considering that besides acting synergistically with CSF, GOHAL can envelop and passivate CSF particles, preventing them to adsorb oxygen species and water contaminants, thus curbing the degradation of BPA via the SET mechanism already described in the Introduction section. It is also not surprising that the highest BPA abatement rate is obtained for a compound with a small content of GOHAL (i.e., 1.4 wt%) with respect to CSF (i.e.,

98.6 wt%). Indeed, as shown in Fig. 1d, GOHAL tends to form porous nanoribbons, which have a specific surface area much larger than that of the dense and compact CSF nanoparticles. The BPA abatement kinetic constant measured for GOT_98.9 % at 50 °C under dark conditions has the same magnitude of those reported for TiO_2 -based photocatalysts under light irradiation [60–63].

3.3. GOT membranes

We deposited continuous GOT membranes with CSF loading of 98.6 % over a polyethersulfone (PES) UF membrane as support, being GOT_98.6 % the most active material in the degradation of BPA. Moreover, membrane layers prepared with CSF loadings higher than 98.6 % after drying showed scarce homogeneity and poor adhesion to the support during handling. The aspect and size of the GOT_98.6 % membranes used in the filtration experiment are depicted in Fig. 3a. A collection of SEM micrographs of a GOT_98.6 % membranes at different magnifications is shown in Fig. 3(b–e). The surface of the membrane appears to be continuously coated by the GOT_98.6 % layer (Fig. 3b). Although channels and inhomogeneities appear on the membrane surface, GOT_98.6 % membranes still present good rejection towards BPA and organic matter, as will be discussed in Sections 3.4 and 3.5. The thickness of the active layer is very limited and not easily measurable given the intimate interaction with the support, as visible in Fig. 3c. At higher magnification (Fig. 3d), it is evident that the active phase is layered on the top of the support, with GOHAL covering the PES support and embedding CSF aggregates. The contrast shown by the secondary electron image (Fig. 3e) well reproduce what is visible in the back-scattered electron images (not reported for brevity) and the EDS analysis confirms that part α of the membrane is essentially composed by GOHAL, with signals related to the presence of carbon and oxygen atoms (atomic percentage C = 72.67 ± 8.21 , O = 23.43 ± 9.58); whereas part β is essentially composed by Sr, Fe and O atoms (atomic % Sr = 12.38 ± 5.39 , Fe = 18.16 ± 1.87 , O = 53.42 ± 10.10). Hence, the Sr/Fe atomic ratio measured in β is compatible with the nominal composition of CSF. Ce atoms are also detected by EDS, but it is not possible to quantify this element, due to the low concentration. EDS also shows the presence of impurities of S and Cl, as confirmed by XPS analysis (see Section 3.5). S impurities probably derive from the Hummers' synthesis of GO, whereas Cl impurities come from the HCl used to promote chemical crosslinking of GOHAL.

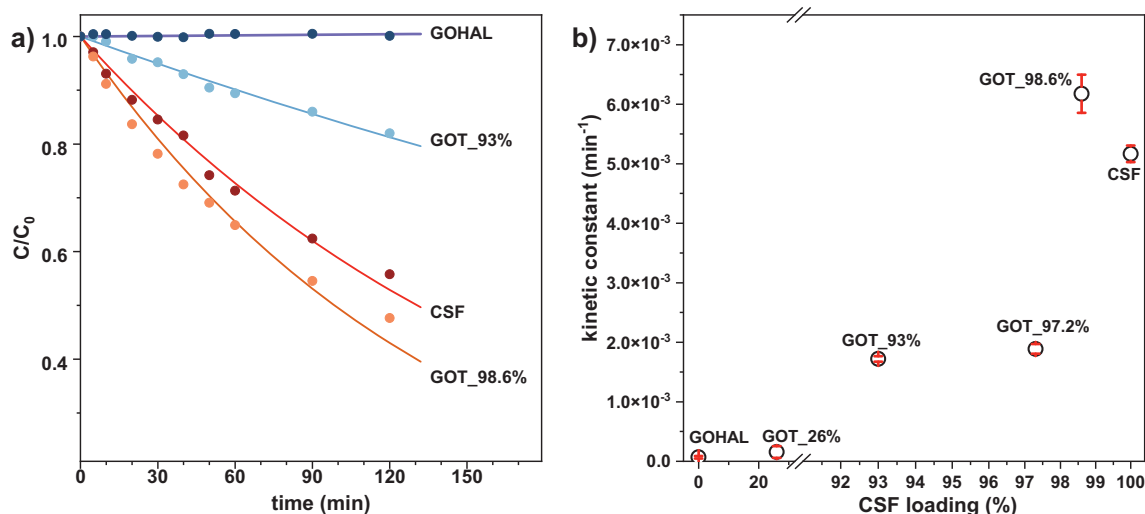


Fig. 2. (a) Relative concentration of BPA (C/C_0) as a function of the time for selected GOT nanocomposites (experimental conditions are described in Section 2.6). The lines in the graph indicate the fitting of the pseudo-first order kinetic model over the experimental points; (b) the pseudo-first order kinetic constants (k) as a function of the CSF loading in the GOT nanocomposites.

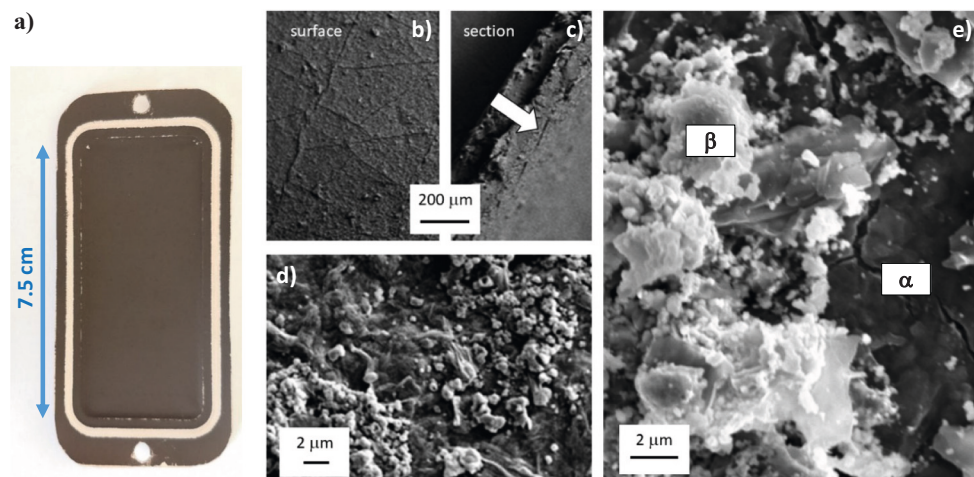


Fig. 3. GOT_98.6 % membrane: (a) macroscopic aspect and size of an operating GOT_98.6 % membrane and (b–e) SEM images of the membrane at different magnifications. Low magnification images of surface (b) and cross-section (c), the arrow evidence the active layer on the top of the PES support (d–e) high magnification micrograph of the surface, where α and β indicate the positions chosen for EDS analysis.

3.4. Bisphenol A rejection and abatement by GOT_98.6 % membranes

The PES support, three GOT_98.6 % membranes, and a GOHAL reference sample (prepared with the same method used for the nanocomposite membranes) were tested in a crossflow nanofiltration apparatus to evaluate their water permeance, their rejection of BPA, the ability of CSF to oxidize BPA molecules in the retentate when immobilized on the membrane surface, and the reproducibility of GOT membrane performances. The PES support used in this study is a commercial ultrafiltration membrane with MWCO of 100 kDa and water permeance of about $100 \text{ L m}^{-2} \text{ h}^{-1} \text{ bar}^{-1}$. Fig. 4a shows that water permeance drops down to 0.8 and $1.3 \text{ L m}^{-2} \text{ h}^{-1} \text{ bar}^{-1}$ after coating with GOHAL and GOT_98.6 % layers, respectively. It is surprising that GOT_98.6 % membrane, which largely consists of dense ceramic particles, has higher permeance than the GOHAL reference, which is entirely made of a water-permeable material, i.e., HAL-crosslinked GO. However, water permeation across GO-based membranes is a complex process [64], involving different paths and mechanisms, including the nearly

“frictionless” transport in nanocapillaries between non-oxidized regions of stacked graphene oxide sheets and the flow through wrinkles and nanopores at the sides of GO nanosheets. Therefore, different phenomena can explain the increased water permeability upon the addition of CSF to GOHAL. For instance, GO sheets tend to align parallelly to the membrane surface creating a high-tortuosity path for the permeation of water molecules. On the contrary, in GOT_98.6 % the GOHAL ribbons are bonded to the surface of the CSF particles (Fig. 1d) and GO nanochannels can assume different orientations, reducing the tortuosity of the permeation path. The ability of GOT membranes for simultaneous BPA abatement and clean water production is here evaluated (Fig. 4b). In a typical filtration experiment, the feed containing 10 mg L^{-1} of BPA in deionized water was kept at 50°C under stirring until the end of the filtration. Regarding the filtration performance, the GOHAL membrane, used as a control experiment in the absence of CSF, retained BPA in the retentate with a selectivity higher than 97 % during all the duration of the filtration. As expected, no degradation of BPA was observed, but BPA concentration remained almost constant in the feed consistently with

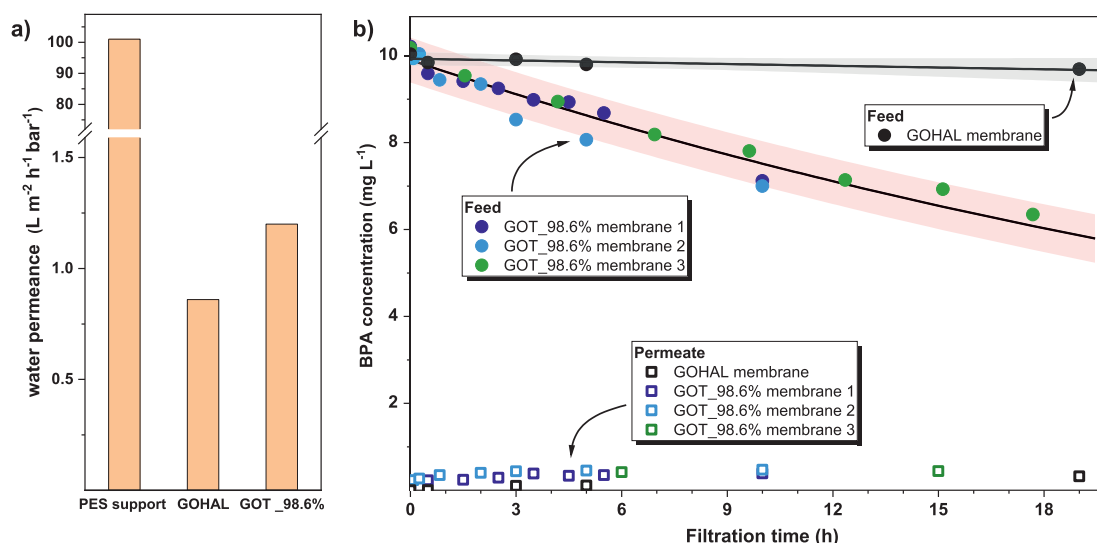


Fig. 4. Filtration tests with model BPA solution (10 g L^{-1} in deionized water): (a) water permeance for the PES support, the GOHAL reference, and GOT_98.6 % membrane; (b) BPA concentration in the feed and the permeate during filtration with the reference GOHAL and 3 different GOT_98.6 % membranes: “membrane 1” and “membrane 2” were fabricated from the same GO and CSF batches, while “membrane 3” was prepared from separate GO and CSF batches. Gray and pink areas indicate the 95 % confidence for the fittings of the equation $y = A \exp(-Bx)$ over the experimental points taken for GOHAL and GOT_98.6 %, respectively. (For interpretation of the references to color in this figure legend, the reader is referred to the web version of this article.)

the low recovery factor (about 1.19) achieved in our filtration experiments. Three filtration experiments were performed with three GOT_98.6 % membranes, prepared following the same coating procedure on three PES sheets. The results obtained for the three GOT_98.6 % samples are surprisingly similar (Fig. 4b), which indicates that the membrane fabrication process is reproducible although depending on a manual coating procedure and “membrane 3” was prepared using materials from different batches than “membrane 1” and “membrane 2”. Indeed, all the three GOT_98.6 % membranes show the ability to retain and degrade BPA during filtration, owing the thermocatalytic activity of the membrane material observed in Fig. 2. Moreover, the concentrations of BPA in the feed during the three filtration experiments are plotted in Fig. 4b and can be fitted with good approximation ($R^2 = 0.93$) with the equation $y = 9.9 \pm 0.1 \exp \{(-0.027 \pm 0.002) x\}$, which stress the high reproducibility of the GOT_98.6 % membranes presented in this work. Additionally, GOT_98.6 % membranes present good selectivity towards BPA, indicating that the coated layers are enough continuous and with a sufficiently limited defect density efficiently reject BPA, although the SEM images in Fig. 3 show some inhomogeneities on the membrane surface. The BPA concentration of the initial feeds in the three experiments was measured to be $10.19 \pm 0.03 \text{ mg L}^{-1}$, while the BPA concentration in the permeate remained nearly constant at $0.33 \pm 0.09 \text{ mg L}^{-1}$. This observation suggests that during crossflow filtration the GOT_98.6 % active layer did not undergo relevant changes and the membranes continued producing a clean permeate. However, it should also be noticed that, while the permeate

composition remained constant during filtration, the concentration of the BPA in the feed dropped from about 10.2 mg L^{-1} at the beginning of the experiment to about 6 mg L^{-1} after 18 h, due to the thermocatalytic abatement of the pollutant. Therefore, the selectivity of the membrane decreased from 97 % to 94 %, according to Eq. (1). Different phenomena can generate this decrement in selectivity, including adsorption and concentration polarization of BPA at the membrane surface. However, we cannot exclude that GOT_98.6 % membranes were affected by the crossflow conditions used in these experiments with the formation of small defects, which slightly reduced the selectivity of the membrane. This aspect should be investigated in future studies.

3.5. Antifouling properties

The ability of the thermocatalytic GOT_98.6 % membrane to retain the non-toxic organic matter and to mitigate fouling was investigated by filtering the effluent collected from an urban wastewater treatment plant. The collected wastewater samples had a starting total organic carbon concentration (TOC) of about 50 mg L^{-1} and it was fed to the membranes at a temperature of 50°C . Fig. 5a shows the permeate flux as a function of the time when filtering the wastewater effluent on a GOT_98.6 % membrane and the GOHAL reference. For both membranes, the flux of the permeate (J_p) decreases along the filtration time, which is typical for fouled membranes. However, in the case of the GOHAL, J_p starts from $4.6 \text{ L m}^{-2} \text{ h}^{-1}$ and drops to $2.8 \text{ L m}^{-2} \text{ h}^{-1}$ after 24 h of filtration time, while the permeate flux of GOT_98.6 % decreases only

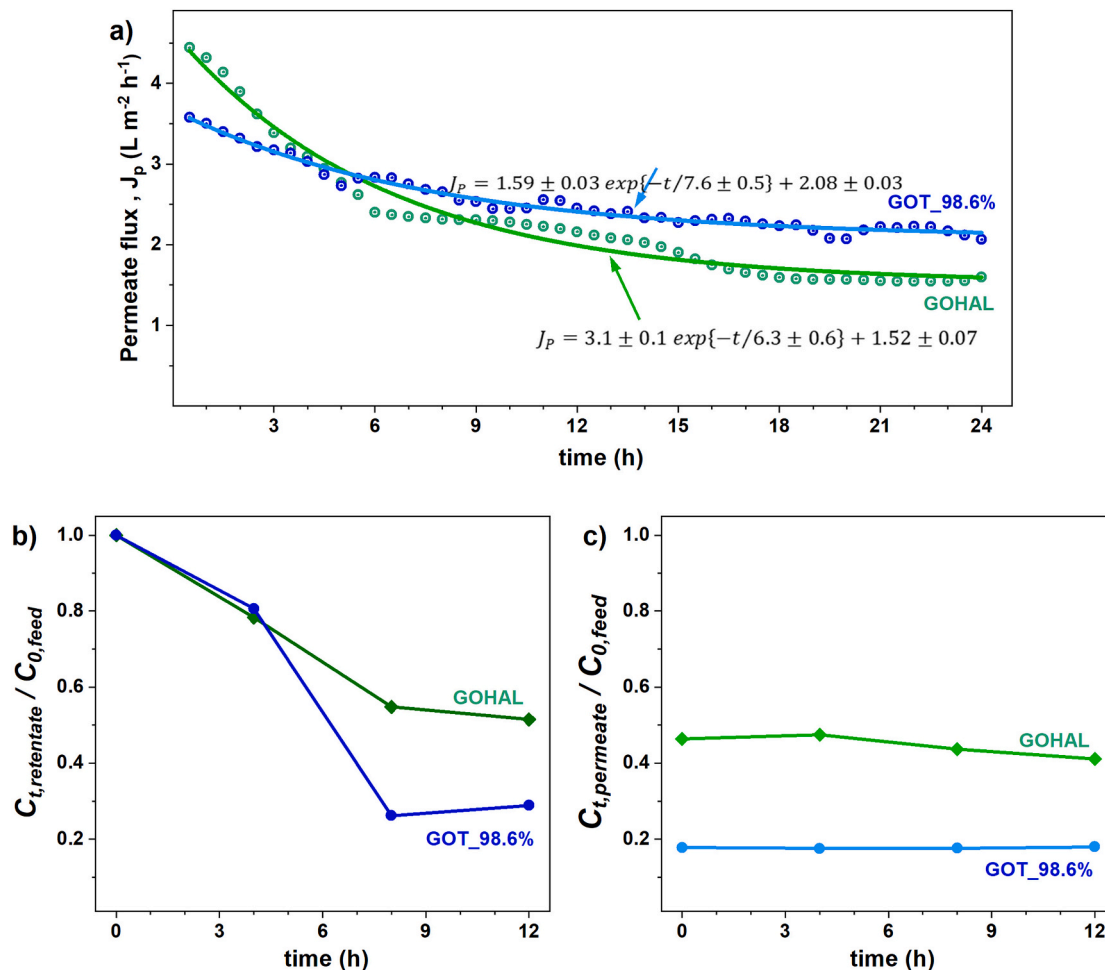


Fig. 5. Filtration of a wastewater plant effluent over GOT_98.6 % and GOHAL membranes: (a) Permeate flux (J_p) as a function of the filtration time, experimental points (bullets), and exponential decay fittings (lines), whose equations are reported in the graph; (b) total organic carbon (TOC) of the feed as a function of the filtration time; (c) TOC of the permeate as a function of the time. Experimental conditions are described in detail in Section 2.7.

from $3.7 \text{ L m}^{-2} \text{ h}^{-1}$ to $2.1 \text{ L m}^{-2} \text{ h}^{-1}$. The lower decrement of permeate flow for GOT_98.6 % than GOHAL can be ascribed to the thermocatalytic properties of the first membrane. Indeed, GOT_98.6 % mitigates fouling by partially degrading the organic matter deposited on the membrane surface. To confirm this hypothesis, TOC of the retentate ($C_{t,retentate}$) and permeate ($C_{t,permeate}$) samples were measured at different filtration times. Fig. 5b shows the TOC of the retentate relatively to the starting TOC of the wastewater effluent fed to the membrane. Surprisingly in both cases, we observed a drop of the TOC concentration in the feed solutions during filtration. In the case of the GOHAL membrane, which is characterized by a passive filtration layer, TOC abatement can be attributed to adsorption of organic molecules on the membrane surface, which is caused by water permeation through the membrane and by the chemical similarity of GOHAL with the dissolved humic substances and is consistent with the J_p decline observed in Fig. 5a. The TOC in the feed of GOT_98.6 % presents a higher decrement than GOHAL after 4 h of

filtration time. In this case, TOC abatement can be caused both by the adsorption on the membrane surface and by the thermocatalytic degradation of the organic matter. The ability of GOT_98.6 % to degrade organic matter can explain the lower tendency to fouling than GOHAL, as observed in Fig. 5a. Moreover, Fig. 5c shows that the GOT_98.6 % can produce a cleaner permeate (lower TOC) than GOHAL.

X-Ray Photoelectron Spectroscopy was used to analyze the changes on membrane surface after 24 h of filtration. Fig. 6A and B shows the survey spectra of the GOHAL and GOT_98.6 % fresh and after filtering the wastewater effluent for 24 h under crossflow conditions. The fresh membranes present the peaks attributable to C and O, typical of oxidized graphene. However, we can observe also small peaks related to Na (Na1s binding energy = 1072 eV), Cl (Cl2p = 198.6 eV), and S (S2p = 169.5 eV) which are probably residues of the reagents used in the extraction of HAL, the synthesis of GO, and for the membrane crosslinking and curing process, respectively (according to the procedures in Sections 2.2, 2.3,

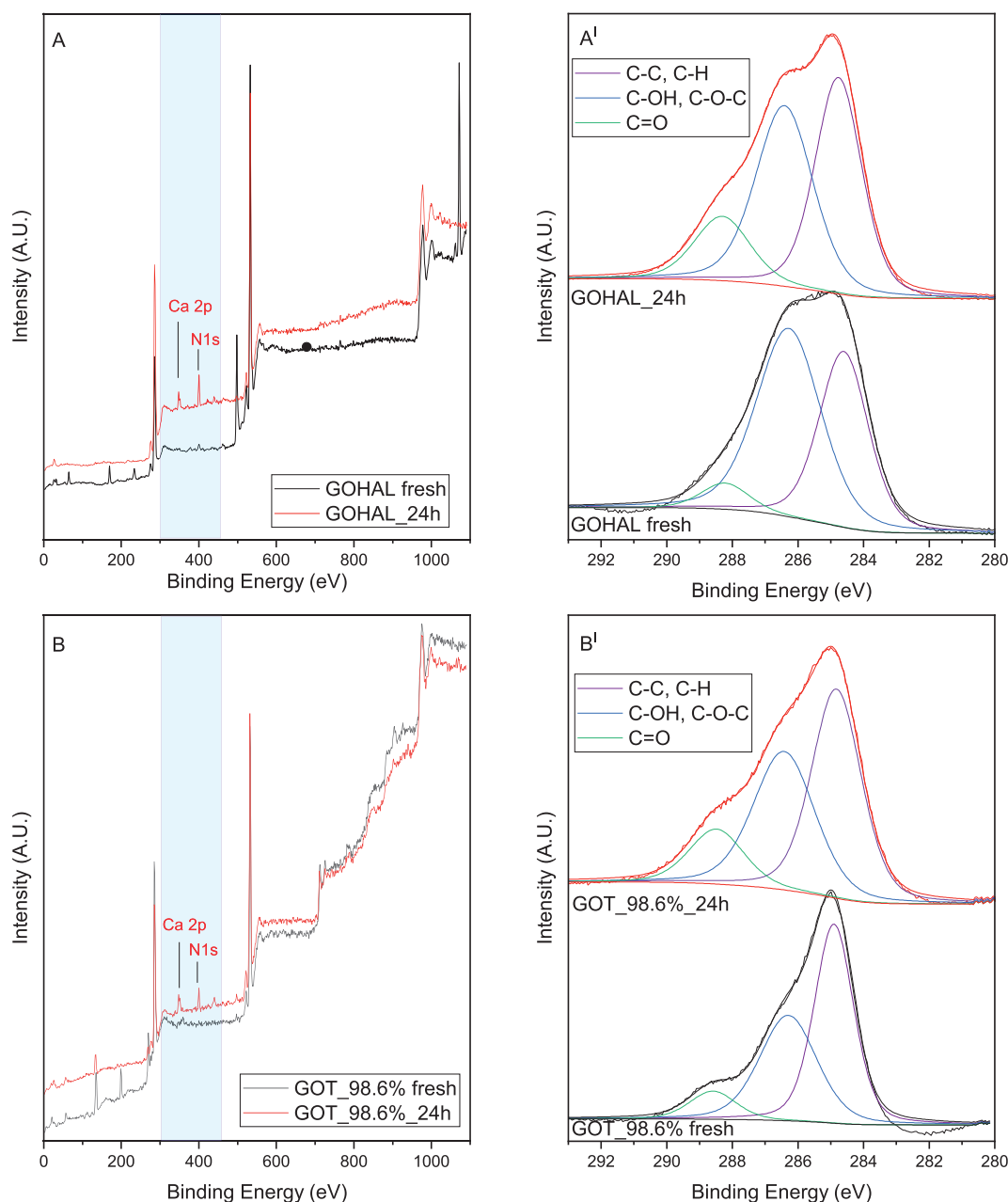


Fig. 6. XPS analysis of the membrane surfaces fresh and after 24 h of filtration: (A) survey spectra of GOHAL; (B) survey spectra of GOT_98.6 %; (A') C1s region of GOHAL; (B') C1s region of GOT_98.6 %.

and 2.4). After filtration, the signals relative to these elements disappear, as expected since these impurities are weakly bonded to the membrane material and ready to be washed out during filtration. On the other hand, two new peaks appear after filtration, namely $\text{Ca}2p$ and $\text{N}1s$. The $\text{Ca}2p$ peak can be ascribed to scaling, i.e., precipitation of CaCO_3 on the membrane surface. The $\text{N}1s$ peak is centered at 400 eV, which is a typical value for organic nitrogen compounds [65], indicating the deposition of organic and biological substances on the membrane surface during filtration, i.e., fouling. These findings confirm the capacity of both membranes to partially retaining both the inorganic and organic components of the wastewater feed. Nevertheless, the N/Ca atomic ratio is 2.8 for GOT_98.6 % and 3.6 for the GOHAL reference. The lower concentration of organic N on the membrane surface for the GOT_98.6 % confirms the antifouling properties of this membrane due to the thermocatalytic activity of CSF, which was observed in Fig. 5a.

The fresh GOT_98.6 % also shows the characteristic signals of Sr ($\text{Sr}3d5/2 = 134.1$ eV), Fe ($\text{Fe}2p3/2 = 710.9$ eV), and Ce ($\text{Ce}3d5/2 = 882.1$ eV), confirming the presence of CSF [66]. The binding energies of the different components of $\text{C}1s$ peaks are shown in Fig. 6A' and B' for GOHAL and GOT_98.6 % respectively. In both cases components relative to graphitic carbon (C—C and C—H at 284.6 eV) oxidized carbon (C—OH and C—O—C at 286.3 eV) and carboxyl groups (C=O at 288.5 eV) are present. By comparing the C distribution between GOHAL and GOT_98.6 % a notable decrease of the relative amount of C—OH, C—O—C component is seen suggesting an interaction of the CSF with the hydroxyl groups of the GO. After filtration, the component relative amount of C=O increases due to the deposition of oxidized organic matter [54,65].

3.6. Toxicological studies with aquatic model organisms

Aquatic model organisms from different trophic levels were exposed to CSF particles to assess the potential ecotoxicity of the membrane perovskite if released into the environment. The short-term toxicity of hazardous substances to aquatic organisms was classified based on LC_{50} and EC_{50} values [67]. Substances with EC_{50} values >10 mg L^{-1} in acute toxicity tests belong to the group with the least apparent ecotoxicity and are not considered very harmful in the environment [67]. This was the case for the two CSFs tested in the current study. Indeed, Table 1 shows that the acute toxicity at 20 °C for 3 model organisms is low with median effective concentrations (EC_{50}) above 50 mg L^{-1} for the green microalgae *R. subcapitata* and the zooplankton organism *D. magna*. The apparent EC_{50} for the luminescent bacterium *A. fischeri* was above 100 mg L^{-1} .

The ecotoxicity potential of the thermocatalytic perovskite CSF material is likely temperature-dependent and additional toxicity assays were therefore conducted with *D. magna* at four incubation temperatures (10, 20, 25, and 30 °C). The results showed that short-term toxicity (0–48 h) of the CSF material at concentrations between 0.5 and 50 mg L^{-1} was negligible regardless of incubation temperature (Fig. 7). At very

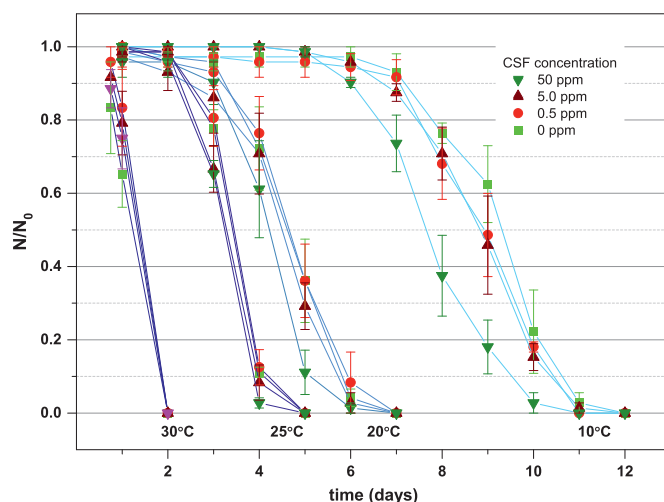


Fig. 7. Starvation survival of *D. magna* exposed to CSF powder at four temperatures (10, 20, 25 and 30 °C). The number of surviving animals at different time points (N) is expressed relative to the number of live animals at the beginning of the experiment (N_0).


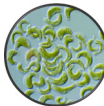
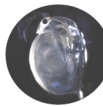
stressful conditions where test animals were incubated >48 h without access to a food source (starvation-survival), the highest CSF concentrations (50 mg L^{-1}) resulted in somewhat decreased survival at 10 °C relative to control samples (Fig. 7). The median survival times (SS_{50}) for *D. magna* at 10 °C was 9.3 days in the absence of CSF material whereas incubation with 50 mg L^{-1} CSF resulted in SS_{50} values of 7.7 and 8.2 days, respectively. The differences for 50 mg L^{-1} were not statistically significant for all time points at 10 °C ($p > 0.05$) and effects were not observed at the more environmentally relevant exposure concentrations of 0.5 and 5 mg L^{-1} . No effects of the CSF material relative to control samples were observed at elevated temperatures of 25 and 30 °C regardless of exposure concentration (Fig. 7).

4. Conclusions

A novel thermocatalytic nanofiltration membrane was prepared by a simple coating procedure, which allowed embedding a perovskite with composition $\text{Sr}_{0.85}\text{Ce}_{0.15}\text{FeO}_{3-\delta}$ (CSF) in a crosslinked graphene oxide matrix. The new membrane material (GOT) demonstrated the benefit of coupling the thermocatalytic perovskite with crosslinked graphene oxide in terms of both CECs abatement and processability. A GOT membrane containing 98.6 wt% CSF is the best compromise to improve the material efficiency in water depollution without blocking the active surface sites of the perovskite. Moreover, a material with such composition is suitable for coating continuous films over a commercial PES support. The GOT_98.6 % membranes prepared in this study showed selectivity and water permeability in the nanofiltration range. When used at 50 °C, GOT_98.6 % membranes were able to retain and degrade BPA in a model solution and to mitigate fouling while filtering a real wastewater plant effluent. GOT membranes are prepared by a highly reproducible method, which does not require organic solvents in any step from the synthesis of the starting materials (i.e., GO, HAL and CSF) to the deposition of the filtering layer. Additionally, we provided experimental evidence of the low toxicity of the thermocatalytic material towards aquatic organisms. A major drawback of the membrane is the need to operate at temperatures higher than ambient in order to achieve appreciable abatement rates. However, many industrial wastewaters either have already a temperature suitable for GOT activation or can be heated on site by low-grade waste heat with no additional costs. Moreover, in many geographical areas solar thermal energy can be exploited for the heating of the wastewater stream fed to the membrane. Long term stability of GOT membranes under real operation conditions

Table 1

EC_{20} and EC_{50} for the CSF powder in toxicity tests with three aquatic model organisms at 20 °C.

<i>A. fischeri</i> (30 min)		<i>R. subcapitata</i> (72 h)		<i>D. magna</i> (48 h)	
					
EC_{20} mg L^{-1}	EC_{50} mg L^{-1}	EC_{20} mg L^{-1}	EC_{50} mg L^{-1}	EC_{20} mg L^{-1}	EC_{50} mg L^{-1}
59.8	>100	19.7	>50	>50	>50

needs to be demonstrated as well. Despite these concerns, the reported thermocatalytic GOT membranes present simultaneous functionalities with no need for additional chemicals and light sources. These functionalities include selectivity in the nanofiltration range, thermocatalytic abatement of organic contaminants, and antifouling properties. Hence, this thermocatalytic membrane has attractive abilities for wastewater treatment.

Declaration of competing interest

The authors declare that they have no known competing financial interests or personal relationships that could have appeared to influence the work reported in this paper.

Acknowledgments

This research has received funding from the European Union's Horizon 2020 research and innovation programme under the Marie Skłodowska-Curie grant agreement 765860 (AQUALity) and from the Eurostars joint programme under the grant agreement E!113844. The authors wish to thank Dr. Davide Palma and Prof. Alessandra Bianco Prevot (Turin University, Italy) for the total organic carbon (TOC) analyses.

References

- [1] B. Petrie, R. Barden, B. Kasprzyk-Hordern, A review on emerging contaminants in wastewaters and the environment: current knowledge, understudied areas and recommendations for future monitoring, *Water Res.* 72 (2016) 3–27.
- [2] Y.K. Tang, Y.X. Zhong, H.L. Li, Y.T. Huang, X.Y. Guo, F. Yang, Y. Wu, Contaminants of emerging concern in aquatic environment: occurrence, monitoring, fate, and risk assessment, *Water Environ. Res.* 92 (2020) 1811–1817.
- [3] M. Patel, R. Kumar, K. Kishor, T. Mlsna, C.U. Pittman, D. Mohan, Pharmaceuticals of emerging concern in aquatic systems: chemistry, occurrence, effects, and removal methods, *Chem. Rev.* 119 (2019) 3510–3673.
- [4] D. Cacace, D. Fatta-Kassinos, C.M. Manaia, E. Cytryn, N. Kreuzinger, L. Rizzo, P. Karaolia, T. Schwartz, C. Merlin, H. Garelick, H. (Schmitt) D. de Vries, C. U. Schwermer, S. Meric, C.B. Ozkal, M.N. Pons, D. Kneis, T.U. Berendonk, Antibiotic resistance genes in treated wastewater and in the receiving water bodies: a pan-European survey of urban settings, *Water Res.* 162 (2019) 320–330.
- [5] A.J. Reid, A.K. Carlson, I.F. Creed, E.J. Eliason, P.A. Gell, P.T.J. Johnson, K.A. Kidd, T.J. MacCormack, J.D. Olden, S.J. Ormerod, J.P. Smol, W.W. Taylor, K. Tockner, J. C. Vermaire, D. Dudgeon, S.J. Cooke, »Emerging threats and persistent conservation challenges for freshwater biodiversity,« *Biol. Rev.* 94 (2019) 849–873.
- [6] P. Nguyen, G. Carvalho, M.A.M. Reis, A. Oehmen, A review of the biotransformations of priority pharmaceuticals in biological wastewater treatment processes, *Water Res.* 188 (2021), 116446.
- [7] I. Michael-Kordatou, C. Michael, X. Duan, X. He, D.D. Dionysiou, M.A. Mills, D. Fatta-Kassinos, Dissolved effluent organic matter: characteristics and potential implications in wastewater treatment and reuse applications, *Water Res.* 77 (2015) 213–248.
- [8] D.B. Miklos, C. Remy, M. Jekel, K.G. Linden, J.E. Drewes, U. Hübner, Evaluation of advanced oxidation processes for water and wastewater treatment – a critical review, *Water Res.* 139 (2018) 118–131.
- [9] L. Rizzo, S. Malato, D. Antakyali, V.G. Beretsou, M.B. Dolic, W. Gernjak, E. Heath, I. Ivancev-Tumbas, P. Karaolia, A.R.L. Ribeiro, G. Mascolo, C.S. McArdell, H. Schaar, S.A.M. T, F.-K. D, Consolidated vs new advanced treatment methods for the removal of contaminants of emerging concern from urban wastewater, *Scienze of the Total Environment* 655 (2019) 986–1008.
- [10] A.R.L. Ribeiro, N.F.F. Moreira, G.L. Puma, A.M.T. Silva, Impact of water matrix on the removal of micropollutants by advanced oxidation technologies, *Chem. Eng. J.* 363 (2019) 155–173.
- [11] P.R. Rout, T.C. Zhang, P. Bhunia, R.Y. Surampalli, in: *Treatment Technologies for Emerging Contaminants in Wastewater Treatment Plants: A Review* 753, 2021, p. 141990.
- [12] R.C. Xiao, Y.G. Wei, D. An, D.L. Li, X.X. Ta, Y.H. Wu, Q. Ren, A review on the research status and development trend of equipment in water treatment processes of recirculating aquaculture systems, *Rev. Aquacult.* 11 (3) (2019) 863–895.
- [13] V. Boffa, D. Fabbri, P. Calza, D. Revelli, P.V. Christensen, Potential of nanofiltration technology in recirculating aquaculture systems in a context of circular economy, *Chem. Eng. J. Adv.* (2022) 100269.
- [14] M.H. Zhang, H. Dong, L. Zhao, D.X. Wang, D. Meng, A review on Fenton process for organic wastewater treatment based on optimization perspective, *Sci. Total Environ.* 670 (2019) 110–121.
- [15] X.C. Liu, Y.Y. Zhou, J.C. Zhang, L. Luo, Y. Yang, H.L. Huang, H. Peng, L. Tang, Y. Mu, Insight into electro-Fenton and photo-Fenton for the degradation of antibiotics: mechanism study and research gaps, *Chem. Eng. J.* 347 (2018) 379–397.
- [16] A. Serra, L. Philippe, F. Perreault, S. Garcia-Segura, Photocatalytic treatment of natural waters. Reality or hype? The case of cyanotoxins remediation, *Water Res.* 188 (2021), 116543.
- [17] J.J. Rueda-Marquez, I. Levchuk, P.F. Ibanez, M. Sillanpaa, A critical review on application of photocatalysis for toxicity reduction of real wastewaters, *J. Clean. Prod.* 258 (2020), 120694.
- [18] H. Chen, J. Motuzas, W. Martens, J. Diniz da Costa, Degradation of azo dye Orange II under dark ambient conditions by calcium strontium copper perovskite, *Appl. Catal. B Environ.* 221 (2018) 691–700.
- [19] H. Chen, J. Motuzas, W. Martens, Surface and catalytic properties of stable Me(Ba, Ca and Mg)SrCoO₃, *Appl. Surf. Sci.* 450 (2018) 292–300.
- [20] H. Chen, J. Motuzas, W. Martens, J.C.D.d. Costa, Ceramic metal oxides with Ni²⁺ active phase for the fast degradation of Orange II dye under dark ambient, *Ceram. Int.* 44 (2018) 6634–6640.
- [21] X. Sun, J. Lin, Synergetic effects of thermal and photo-catalysis in purification of dye water over SrTi_{1-x}MnxO₃ solid solutions, *J. Phys. Chem. C* 113 (12) (2009) 4970–4975.
- [22] H. Chen, J. Ku, L. Wang, Thermal catalysis under dark ambient conditions in environmental remediation: fundamental principles, development, and challenges, *Chin. J. Catal.* 40 (2019) 1117–1134.
- [23] M. Tummino, E. Laurenti, F. Deganello, A.B. Prevot, G. Magnacca, Revisiting the catalytic activity of a doped SrFeO₃ for water pollutants removal: Effect of light and temperature, *Appl. Catal. B Environ.* 207 (2017) 174–181.
- [24] K. Janowska, V. Boffa, M.K. Jørgensen, C.A. Quist-Jensen, F. Hubac, F. Deganello, F.E.B. Coelho, G. Magnacca, Thermocatalytic membrane distillation for clean water production, *npj Clean Water* 1 (3) (2020) 34.
- [25] K.J. Janowska, X. Ma, V. Boffa, M. Jørgensen, V. Candelario, Combined nanofiltration and thermocatalysis for the simultaneous degradation of micropollutants, fouling mitigation and water purification, *Membranes* 11, 8 (2021) 639.
- [26] X. Ma, Q.-J.C. A, A. Ali, B. V, Desalination of groundwater from a well in Puglia Region (Italy) by Al₂O₃-doped silica and polymeric nanofiltration membranes, *Nanomaterials* 10 (9) (2020) 1738.
- [27] B. V, Inorganic materials for upcoming water purification membranes, in: *Current Trends and Future Developments on (Bio-) Membranes: Membrane Technology for Water and Wastewater Treatment - Advances and Emerging Processes*, Elsevier (S&T), 2020, pp. 117–140.
- [28] W.S. Koe, J.W. Lee, W.C. Chong, Y.L. Pang, L.C. Sim, An overview of photocatalytic degradation: photocatalysts, mechanisms, and development of photocatalytic membrane, *Environ. Sci. Pollut. Res.* 27 (3) (2020) 2522–2565.
- [29] S.W. Leong, A. Razmjou, K. Wang, K. Hapgood, X.W. Zhang, H.T. Wang, TiO₂ based photocatalytic membranes: a review, *J. Membr. Sci.* 472 (2014) 167–184.
- [30] H. Zhang, J.Q. Luo, J.M. Woodley, Y.H. Wan, Confining the motion of enzymes in nanofiltration membrane for efficient and stable removal of micropollutants, *Chem. Eng. J.* 421, 2 (2021), 127870.
- [31] J. Wang, L.J. Qin, J.Y. Lin, J.Y. Zhu, Y.T. Zhang, J.D. Liu, B. Van der Bruggen, Enzymatic construction of antibacterial ultrathin membranes for dyes removal, *Chem. Eng. J.* 323 (2017) 56–63.
- [32] P. Karaolia, I. Michael-Kordatou, E. Hapeshi, C. Drosou, Y. Bertakis, D. Christofilos, G.S. Armatas, L. Sygellou, T. Schwartz, N.P. Xekoukoulotakis, D. Fatta-Kassinos, Removal of antibiotics, antibiotic-resistant bacteria and their associated genes by graphene-based TiO₂ composite photocatalysts under solar radiation in urban wastewaters, *Appl. Catal. B Environ.* 224 (2018) 810–824.
- [33] Y. Gao, M. Hu, B. Mi, Membrane surface modification with TiO₂-graphene oxide for enhanced photocatalytic performance, *J. Membr. Sci.* 455 (2014) 349–356.
- [34] M.L. Tran, C.C. Fu, L.Y. Chiang, C.T. Hsieh, S.H. Liu, R.S. Juang, Immobilization of TiO₂ and TiO₂-GO hybrids onto the surface of acrylic acid-grafted polymeric membranes for pollutant removal: analysis of photocatalytic activity, *J. Environ. Chem. Eng.* 8, 5 (2020), 104422.
- [35] F. Cesano, V. Boffa, F.E.B. Coelho, G. Magnacca, Graphene and graphene-oxide for enhancing the photocatalytic properties of materials, in: « i Materials Science in Photocatalysis, Elsevier, 2021, pp. 385–396.
- [36] R.L. Liu, M. Zhao, X.Y. Zheng, Q. Wang, X.F. Huang, Y. Shen, B.L. Chen, Reduced graphene oxide/TiO₂(B) immobilized on nylon membrane with enhanced photocatalytic performance, *Sci. Total Environ.* 799 (2021), 149370.
- [37] K.P. Gopinath, N.V. Madhav, A. Krishnan, Present applications of titanium dioxide for the photocatalytic removal of pollutants from water: a review, *J. Environ. Manag.* 270 (2020) 11090.
- [38] H. Qu, X. Xiao, Z. Han, M. Hu, S. Shen, L. Yang, F. Jia, T. Wang, Z. Ye, W. Sun, Y. Wang, L. Huang, Z. Zhu, P. Servati, J. Tang, J. Chen, Graphene oxide nanofiltration membrane based on three-dimensional size-controllable metal-organic frameworks for water treatment, *ACS Appl. Nano Mater.* 5 (4) (2022) 5196–5207.
- [39] Z. Zhang, X. Xiao, Y. Zhou, L. Huang, Y. Wang, Q. Rong, Z. Han, H. Qu, Z. Zhu, S. Xu, J. Tang, J. Chen, Bioinspired graphene oxide membranes with pH-responsive nanochannels for high-performance nanofiltration, *ACS Nano* 15 (8) (2021) 13178–13187.
- [40] Z. Han, X. Xiao, H. Qu, M. Hu, C. Au, A. Nashalian, X. Xiao, Y. Wang, L. Yang, F. Jia, T. Wang, Z. Ye, P. Servati, L. Huang, Z. Zhu, J. Tang, J. Chen, Itrafast and selective nanofiltration enabled by graphene oxide membranes with unzipped carbon nanotube networks, *ACS Appl. Mater. Interfaces* 14 (1) (2022) 1850–1860.
- [41] Y. Du, L. Huang, X. Wang, et al., Preparation of graphene oxide/silica hybrid composite membranes and performance studies in water treatment, *J. Mater. Sci.* 55 (2020) 11188–11202.

- [42] K. Yang, L.-J. Huang, Y.-X. Wang, Y.-C. Du, Z.-J. Zhang, Y. Wang, M. Kipper, L. Belfiore, J.-G. Tang, Graphene oxide nanofiltration membranes containing silver nanoparticles: tuning separation efficiency via nanoparticle size, *Nanomaterials* 10 (2020) 454.
- [43] X. Li, Y. Xu, K. Goh, T.H. Chong, R. Wang, Layer-by-layer assembly based low pressure biocatalytic nanofiltration membranes for micropollutants removal, *J. Membr. Sci.* 615 (2020), 118514.
- [44] H. Zhang, J. Luo, J.M. Woodley, Y. Wan, Confining the motion of enzymes in nanofiltration membrane for efficient and stable removal of micropollutants, *Chem. Eng. J.* 421 (2021) 12787.
- [45] F. Deganello, A.K. Tyagi, Solution combustion synthesis, energy and environment: best parameters for better materials, *Prog. Cryst. Growth Charact. Mater.* 64 (2018) 23–61.
- [46] V. Boffa, H. Etmimi, P.M.H.T.G. Magnacca, Y. Yue, Carbon-based building blocks for alcohol dehydration membranes with disorder-enhanced water permeability, *Carbon* (2017) 458–466.
- [47] Comparison of chemical cross-linkers with branched and linear molecular structures for stabilization of graphene oxide membranes, and their performance in ethanol dehydration, *Ind. Eng. Chem. Res.* (2019) 18788–18797. [ãrg. 58.](#)
- [48] A. Strunck, A. Suri, V.B. Effect of temperature and branched crosslinkers on supported graphene oxide pervaporation membranes for ethanol dehydration, *Nanomaterials* 8 (2020) 1571.
- [49] P. Quagliotto, E. Montoneri, F. Tambone, F. Adani, R. Gobetto, G. Viscardi, Chemicals from wastes: compost-derived humic acid-like matter as surfactant, *Environ. Sci. Technol* 40 (2006) 1686–1692.
- [50] E. Montoneri, V. Boffa, P. Savarino, D.G. Perrone, G. Musso, R. Mendichi, M. R. Chierotti, R. Gobetto, Biosurfactants from urban green waste, *ChemSusChem* 2 (2009) 239–247.
- [51] A. Farsi, V. Boffa, H.F. Qureshi, A. Nijmeijer, L. Winnubst, M.L. Christensen, Modeling water flux and salt rejection of mesoporous γ -alumina and microporous organosilica membranes, *J. Membr. Sci.* 470 (2014) 307–315.
- [52] D. Papagiannaki, C. Medana, R. Binetti, P. Calza, P.R. Effect of UV-A, UV-B and UV-C irradiation of glyphosate on photolysis and mitigation of aquatic toxicity, *Scientific Reports* 10 (1) (2020) 12.
- [53] M. Nielsen, P. Roslev, Behavioral responses and starvation survival of *Daphnia magna* exposed to fluoxetine and propranolol, *Chemosphere* 8–9 (2018) 211.
- [54] J. Park, W. Lee, A study of the correlation between the oxidation degree and thickness of graphene oxides, *Carbon* 189 (2022) 579–585.
- [55] Y. Shen, V. Boffa, I. Corazzari, A. Qiao, H. Tao, Y. Yue, Revealing hidden endotherm of Hummers' graphene oxide during, *Carbon* 138 (2018) 337–347.
- [56] U. Nakhikham, G. Magnacca, A. Qiao, P.K. Kristensen, V. Boffa, Yue, Phenol abatement by titanium dioxide photocatalysts: effect of the graphene oxide loading, *Nanomaterials* 9 (2019) 947.
- [57] U. Nakhikham, V. Boffa, G. Magnacca, A. Qiao, L.R. Jensend, Y. Yue, Mutual-stabilization in chemically bonded graphene oxide–TiO₂ heterostructures synthesized by a sol–gel approach, *RSC Adv.* 7 (2017) 41217–41227.
- [58] H.A.A. Jamjoum, K. Umar, R. Adnan, M.R. Razali, M.N.M. Ibrahim, Synthesis, characterization, and photocatalytic activities of graphene oxide/metal oxides nanocomposites: a review, *Front. Chem.* 9 (2021), 752276.
- [59] M. Anjum, R. Miandad, M. Waqas, F. Gehany, M.A. Barakat, Remediation of wastewater using various nano-materials, *Arab. J. Chem.* 12 (8) (2019) 4897–4919.
- [60] A.e.a. Garg, Photocatalytic degradation of bisphenol-A Using N, Co codoped TiO₂ catalyst under solar light, *Scientific Report* 9 (2019) 765.
- [61] C.Y. Kuo, C.H. Wu, H.Y. Lin, Photocatalytic degradation of bisphenol A in a visible light/TiO₂ system, *Desalination* 256 (2010) 37–42.
- [62] B. Gao, T.M. Lim, D.P. Subagio, T.T. Lim, Zr-doped TiO₂ for enhanced photocatalytic degradation of bisphenol A, *Appl. Catal. A* 375 (2010) 107–115.
- [63] CQQWY, Z.C. Jia, Photocatalytic degradation of bisphenol A in aqueous suspensions of titanium dioxide, *Adv. Mater. Res.* 433–440 (2012) 172–177.
- [64] T.S. Yang, H. Lin, K.P. Loh, B.H. Jia, Fundamental transport mechanisms and advancements of graphene oxide membranes for molecular separation, *Chem. Mater.* 31 (6) (2019) 1829–1846.
- [65] The evolution of oxygen-functional groups of graphene oxide as a function of oxidation degree, *Materials Chemistry and Physics* 278 (2022) 125629.
- [66] ASLSZS, J.C.Yanchun Zhang, *J. Mater. Sci. Mater. Electron.* 32 (2021) 21262–21277.
- [67] U. Nations, Globally Harmonized System of Classification and Labelling of Chemicals (GHS), Ninth revised edition, United Nations, New York and Geneva, 2021.